HYBRID FLAX FIBER-BASED HELICOPTER CABIN DOOR - STATIC AND DYNAMIC TESTING WITH DIGITAL IMAGE CORRELATION

Lukas Gaugelhofer M.Sc. Research Assistant
Jonas John M.Sc. Research Assistant
Manfred Hajek Prof. Dr.-Ing. Professor (ret.)
Ilkay Yavrucuk Prof. Dr. phil. Professor and Department Head
Institute for Helicopter Technology and VTOL
Technical University of Munich, Germany

ABSTRACT

This paper presents the design and experimental testing of hybrid flax fiber-based cabin doors for the EDM Aerotec CoAX coaxial ultralight helicopter. With the goal of developing ecologically sustainable structures for aviation, the new cabin door design has 40.8 % bio-based content using uni- and bidirectional high performance flax fiber prepregs with bio-epoxy resin reinforced with carbon fibers at critical load paths in the structure. The static structural properties as well as the modal and damping characteristics of different flax/carbon hybrid designs are evaluated and compared to the original CFRC cabin door using digital image correlation. The results show that similar structural stiffness is achieved with the FFRC door at the expense of a 29.7 % mass increase, which could be reduced to 19.5 % with a projected fiber volume content of 50 %. Experimentally derived loss factors show the expected high inherent damping of flax fiber-reinforced structures.

NOTATION

BD	bidirectional
CFRC	carbon fiber-reinforced composite
DIC	digital image correlation
FFRC	flax fiber-reinforced composite
FRF	frequency response function
FVC	fiber volume content
PMMA	Polymethylmethacrylat
UD	unidirectional
2D	two-dimensional
3D	three-dimensional
E_V	virtual stiffness
σ	tensile stress
τ	shear stress
η	loss factor
ε	tensile strain
γ	shear strain

INTRODUCTION

Research on biocomposites is driven by their low environmental footprint due to low energy requirements during production (Refs. 1–5). In particular, flax fiber-reinforced composites (FFRC) offer good mechanical properties, vibration damping and lightweight potential (Refs. 6–8) and are already used in the automotive industry for interior panels, also valued for their low density and acoustic properties, tool-friendly processability, and splinter- and fracture-free damage characteristics (Refs. 9, 10). For aviation structures, FFRCs are still in the research stage due to the typically stricter standards and high requirements for strength, stiffness, and operational longevity. However, the good mechanical properties and the possibility to improve the damping characteristics of carbon laminates by flax fiber hybridization combined with aeroelastic tailoring offer a high potential for helicopter structures (Refs. 8,11,12).
One of the main challenges for natural fiber composites is the harsh environment of aviation, such as lightning strikes, temperature and humidity, fungus and UV radiation, which are being investigated within the scope of the federal research project *InteReSt II.* (Ref. 13). A representative helicopter cabin door of the ultralight helicopter EDM Aerotec CoAX is used to investigate these effects and to demonstrate and evaluate the technology concept of hybridizing carbon fiber-reinforced composites (CFRC) and FFRCs with the goal of significantly increasing the use of renewable materials up to 50 % and improving the life cycle of semi-structural aviation components. The second generation of flax fiber based cabin doors benefit from the increased strength and stiffness of the new flax prepreg material with bio-epoxy resin, with a higher strength for flax twill weave of 60 % and for unidirectional flax of 24 % compared to the previous research project *InteReSt* (Ref. 14). There it has already been shown that the application of suitable hybrid composites in the aviation sector is possible and that ecological and economic advantages are emerging with a

Presented at the 49th European Rotorcraft Forum, Bückeburg, Germany, September 05–07, 2023.

significant reduction of the CO_2 footprint (Refs. 15–20). However, challenges such as ensuring consistency and manufacturing quality of FFRC structures remain due to the variability of natural fibers in their properties as well as challenges related to the harsh aviation environment. Therefore, further research in this area is needed to advance the development of these materials for aeronautical applications.

MATERIALS

In the previous research project *InteReSt*, the first FFRC cabin door *E* was designed and manufactured. This door was optimized for the use of flax fibers by increasing the area moment of inertia of the cross sections and reinforcing the critical load paths with carbon fibers. The prepregs used were the flax fiber*FlaxPreg BL 150* from SAS LINEO and the carbon fiber *Sigapreg®C W200-TW2/2-E503/45%* from SGL Group. Based on the results of a comprehensive market research and experimental investigation of the tensile properties of flax fiber-reinforced composites in the following research project *InteReSt II*, the bio-epoxy resin prepregs with unidirectional fibers *Fiberpreg N 120 UD EP4.5S Bio* and twill weave *Fiberpreg N 200 T EP4.5S Bio* were found to have a higher bio content and better mechanical properties (Ref. 14). Doors *A*, *B*, *Bs* and *D* were then manufactured with these flax prepregs reinforced with bidirectional carbon prepreg *Krempel BX45IMP530R45 50K 300* g/m^2, unidirectional *Unipreg 150* g/m^2 with *Panex 35 50k C-fibers* and carbon towpreg *Krempel BX45IMP530R45 50K 300* g/m^2. Cabin door Bs has unlike all other doors a PMMA window glued in the structure with an elastic adhesive. The original CRFC cabin door from the coaxial helicopter is referred to as door *C* and will serve as a reference for the investigations. All of these doors, listed in the table 1, are made from autoclave cured prepregs.

Table 1: Development of cabin doors

Door	Description
A	first version of optimized design (2022)
B	improved design/ manufact. quality (2022)
Bs	B door plus PMMA window (2022)
C	original CFRP reference door
D	latest design with reduced mass (2023)
E	from project InteReSt (2016-2019)

The doors are designed as a double-shell structure, with each shell based on flax prepregs and hybridized with carbon reinforcements, as shown in figure 1 for the UD outer shell and in figure 2 for the BD inner shell. The outer shell has four layers [0°, 45°, 90°, -45°] for doors A, B and Bs and three layers [0°, 60°, -60°] for door D of unidirectional and quasi-isotropic flax prepreg. The inner shell is made from two quasi-isotropic twill weave flax layers [0°, 45°]. Tailored fiber placement (TFP) with carbon, UD and BD carbon fibers reinforce critically high loaded segments as shown in figure 15 in the appendix at the example of door B (Ref. 21).

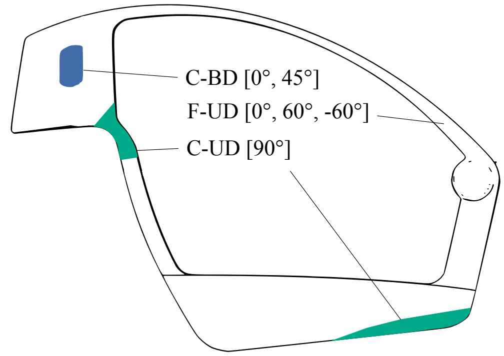

Figure 1: Design of flax fiber-based UD outer shell of cabin door D with carbon fiber reinforcements (Ref. 21)

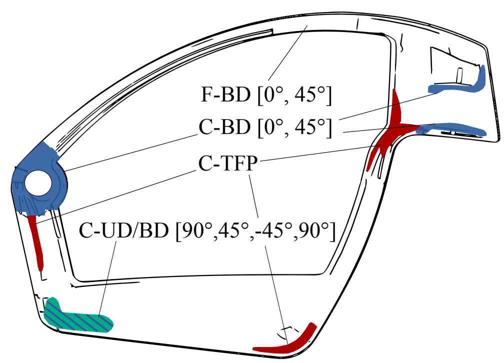

Figure 2: Design of flax fiber-based BD inner shell of cabin door D with CFRC reinforcements and tailored fiber placement (TFP) (Ref. 21)

Geometry differences in door designs

Doors A and E have minor differences in geometry compared to doors B, Bs, C and D as shown in figure 16 in the appendix. The latter have an inward radius at the edges of the outer shell, which can bee also seen at the example of door B in figure 15 in the appendix. In addition, doors A and E have design adaptations regarding small radii of the geometry to avoid sharp bends of the layers as well as the before mentioned increase of area moment of inertia of certain cross sections (Ref. 11).

Door A has no BD carbon patch at the door handle, which results in 21.3 % less carbon content compared to door B and Bs. For the new design of cabin door D, the amount of carbon fibers is reduced by 16.9 % compared to B and Bs by reducing the number of layers of several patches of the reinforcements. Additionally, door D has 26.8 grams of powerRibs™implemented in the outer shell, in order to reduce local buckling of the larger surfaces, which can be seen in figure 18.

Door mass and bio-based content

The total mass at the experimental test, the net mass of the doors, and the total bio content in percent by mass (from net mass) are shown in figure 3. Total mass at test includes adapters required for load applications and the hinge pin. The net mass of the doors consists of the trimmed outer and inner shells plus adhesive, serving as comparable weight between the different designs. The bio content consists of the fraction of flax fibers in the composite and also includes the 22 % bio content of the bio-epoxy resin. Compared to the carbon reference, door B has a higher net mass of 29.7 % with a total bio content of 40.5 %, while door D has a higher net mass of 22.3 % with a total bio content of 40.8 %. The total bio-based content of the doors is dependant on the FVC as well as the bio content of the resin.

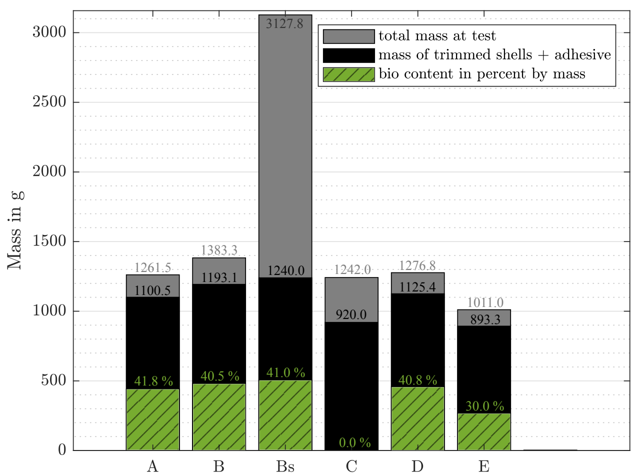

Figure 3: Comparison of total mass at test, net mass and bio-based content of the doors

In particular, the 3D geometry of the inner shell requires good draping qualities of the BD layers and a cutout of the plies divided into several zones as shown in figure 4. However, since the fibers are then cut perpendicular to the direction of the load, an overlap between two zones is required to provide load transfer from one ply to the other.

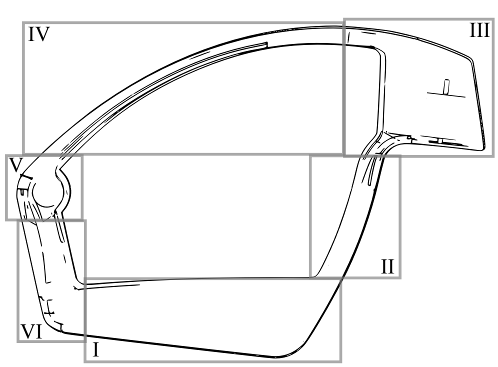

Figure 4: Cutting zones for bi-directional flax fiber prepregs of the inner shell

Cutting optimization of UD prepreg layers

In the case of UD in the outer shell, it is possible to save weight if the cutouts do not overlap. The goal for the new development in door D is to further reduce the weight while maintaining the mechanical properties. By reducing the skin to three layers for door D, the layup requires fiber angles of 0°, 60°, and -60°. In addition, the amount of carbon prepreg is reduced from 141.8 grams (B, Bs) to 117.9 grams (D). Also, to reduce overlap, the UD patches are cut only along the fiber axis, which can then be aligned in the mold. The raw prepreg material from the manufacturer has a width of 700 mm, which results in the optimized cutout for the flat pattern, with the cutting lines of the UD layers shown in red in figure 5.

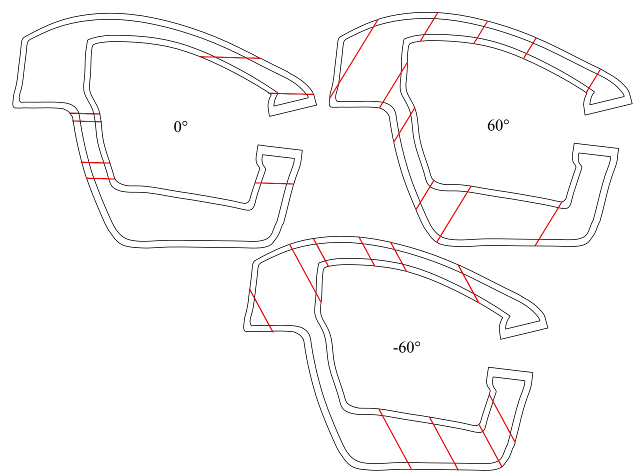

Figure 5: Cutting optimization of outer shell flat pattern for unidirectional flax prepregs of door D

Material properties and curing cycle

The mechanical properties for flax prepregs with epoxy resin with curing cycle *I* (120°C, 5 bar, 2 hours) are available from previous investigations (Ref. 14). However, due to temperature and pressure limitations of the available cabin door molds, a new curing cycle *II* (90°C, 2 bar, 8 hours) has to be applied for the new flax prepreg with bio-based epoxy resin. A tempering process (120°C, 1 hour) in addition to curing cycle *II* is applied on the bio-prepreg test specimens as well as door D. Due to the new curing cycle, it is necessary to characterize the material, which provides data for the finite element analysis of door D. Tensile tests are performed on the UD and BD materials at 0°, 90° and 45° to the fiber direction, which are shown as stress-strain curves in figure 6 for tempered bio-based epoxy prepreg with curing cycle *II* in the green solid line and epoxy prepreg with curing cycle *I* in the blue dash-dotted line. The comparison of an untempered UD0 is shown as black dashed line. The standard deviations SD of tensile stress σ_{11} and σ_{22}, as well as shear stress τ_{12} are shown as semi-transparent areas. The

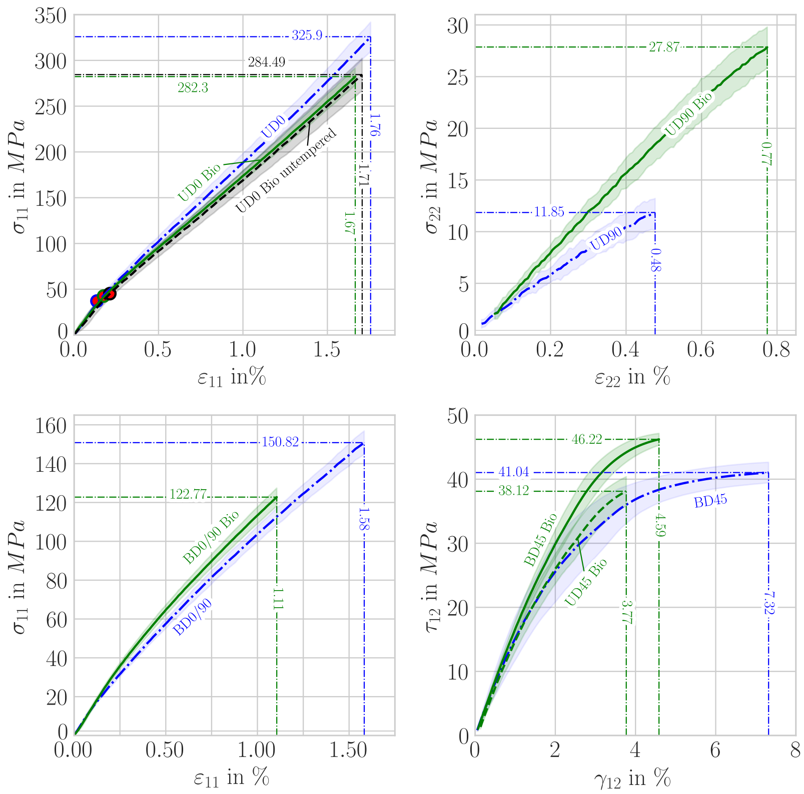

Figure 6: Tensile properties of flax fiber prepregs with bio-epoxy resin

notation of $()_{11}$ refers to parallel to fiber direction and $()_{22}$ perpendicular to fiber direction. The tests are performed on an Instron 4505 in accordance with DIN EN 2561 (UD0) (Ref. 22), DIN EN 2597 (UD90) (Ref. 23), DIN EN 6031 (BD45) (Ref. 24) and DIN EN ISO 527-4 (BD0) (Ref. 25) with a sample size of 7-9 specimens. For $\boldsymbol{\sigma}_{11}$ of UD the yield points between primary and secondary Young's modulus are marked as red dots. Due to the lower autoclave pressure of 2 bar, more resin remains in the composite and therefore the lower FVC of 40.91 % for UD and 40.36 % for BD improves the shear strength by 12.6 % for BD weave. However, the tensile strength $\boldsymbol{\sigma}_{11}$ for FFRC parallel to the fiber direction is reduced by 13.4 % for UD and 18.4 % for BD material. In direction perpendicular to the UD fiber, the lower FVC leads an increase of 135.2 % in $\boldsymbol{\sigma}_{22}$. It must be however noted that apart from the two different curing cycles, also an epoxy resin is compared to a bio-based epoxy resin. The untempered UD0 bio-prepreg shows an increase of 0.77 % in tensile strength and of 2.39 % in elongation at break, leading to a slightly lower stiffness. The tempering process does not show a large influence in fiber direction, however, it allows better processability of the door regarding trimming the edges of inner and outer shell.

Figure 17 in the appendix shows the cured outer shell after demolding, with UD carbon fibers reinforcing a critical load path. The edges of the shells are trimmed bonding with Sika Adekit A170-1/400 (door B, Bs, C, D) or 3M Scotch-Weld EC-9323 (door A and E).

EXPERIMENTAL METHODS

The evaluation of the different cabin door designs is performed by investigating their static mechanical properties and their dynamic behavior. For the static analysis, the door has a fixed support at the hinge pin and a force is applied at the door handle. The displacements of the applied photogrammetric points, distributed over the structure, are measured in three axes with the digital image correlation system *GOM Aramis*. The applied force is measured with a 6-axis load cell *ME K6D130* mounted at the interface between the hinge pin and the wall mount as shown in figure 7. For modal testing, the door structure is excited with an impact hammer and the eigenfrequencies and mode shapes are measured optically via the photogrammetric points at a frame rate of 115 Hz, from which the damping can be evaluated.

Static structural experiments

The purpose of the static measurements is to evaluate the design optimization by comparing several cabin doors. Five load directions in ±X, ±Y, +Z and in three levels L1, L2 and L3 are tested as shown in the table 2. The different load cases simulate e.g. opening, closing and resting of the pilot's arm on the open cabin door. Load level L2 was applied in a previous investigation on door E, which served as a reference (Ref. 11). Load levels L1 and L3 are derived as 50 % and 150 % of L2, respectively. As shown in figure 7, these static loads are applied at point

Table 2: Load levels and directions

Loads	L1 [N]	L2 [N]	L3 [N]
$+X$	3	6	9
$-X$	3	6	9
$+Y$	6	12	18
$-Y$	6	12	18
$+Z$	15	30	45

LA via a cable and pulley system to achieve the different load directions. Due to friction in the pulley, the applied loads have slight variations, which are recorded by the load cell. The optical measurement with the DIC system provides the 3D displacements of the photogrammetric markers in relation to the applied load. Each recorded load case consists of 25 frames taken at a rate of 5 Hz, which makes it possible to apply the average displacement and thus filter the noise. The experimental procedure for a door starts with an unloaded reference, followed by a recording of the unloaded but attached cable before and after each load level. After all load levels of a load direction have been measured, the cable is disconnected and an unloaded reference measurement is taken. Since time-dependant nonlinear creep and creep recovery of the FFRP material is expected (Refs. 26, 27), an additional unloaded reference is recorded after 10 minutes in order to quantify the recovery after creep of the flax fiber composite structure, the results of which are shown in figure 13.

The test setup is shown in figure 7, with the DIC system in front, a calibration cross behind the cabin door as a reference and a load cell at the fixed support of the door. The displacement vectors in the z-axis of each marker can be seen under static load application in +Z.

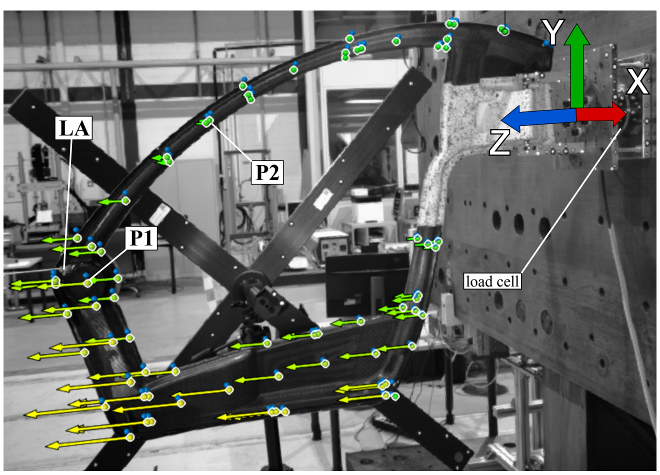

Figure 7: Displacement vectors in z-axis under static load application in +Z with points LA and P1, P2

Experimental modal analysis

For the dynamic measurements, the cabin doors are set up in the same way as for the static structural tests with a fixed support at the hinge pin. The door is excited with an impact hammer at the load application point LA, triggering the DIC system for an image sequence of 13 seconds at a frame rate of 115 Hz. In order to excite different mode shapes, the structure is impacted in -X, -Y and -Z direction. For this dynamic measurement, the integrated light source and reflective markers are required due to the higher shutter speed. The FRF can be obtained from each photogrammetric marker as a displacement in all three dimensions, resulting in a well resolved visualization of the doors's mode shapes, which helps to identify and assign the corresponding eigenfrequencies. In addition, the load cell recorded each event at a sampling rate of 1000 Hz. For the evaluation of the loss factor, the DIC data from points P1 and P2 are combined with the load cell data each with excitation in -X, -Y and -Z. Points P1 and P2 are shown in figure 7. The loss factor η is determined using the half-power bandwidth method of the retrieved FRFs. The maximum frequency at which the signal can be evaluated is half the sampling frequency (Ref. 28). With a sampling frequency of 115 Hz for the DIC system and 1000 Hz for the load cell, this is 57.5 Hz and 500 Hz, respectively. The fixed support of the setup must be considered in the evaluation of the damping because of its influence on the damping.

EXPERIMENTAL RESULTS

The results of the static and dynamic experiments compare the influence of the different designs and used materials on the mechanical and modal characteristics of the doors.

Static structural results

The evaluation and comparison between the doors is made using a virtual stiffness E_v that relates the applied resultant force to the resultant displacement in Newtons per millimeter of point *P1*, which is located in the center of the door handle. A higher E_v is aimed for the improved designs of the cabin door structure. As the CFRP cabin door C is the original door used in the CoAX helicopter, it is used as a reference. Figure 8 shows the results for the applied force in +X, equivalent to the direction of closing the cabin door. Due to the lower torsional stiffness of a different hinge pin, which was used in doors Bs and C, the results cannot be compared for the load cases +X and -X. The results for +X show that door E has the lowest E_v. Door B has the highest virtual stiffness, followed by door D, which has three UD layers in the outer shell compared to four layers in door B. With door A having nearly the same layup as door B except for less carbon fibers around the door handle, the lower virtual stiffness could be attributed to the different geometry of the outer shell with the inwards radius that increases the area moment of inertia as shown in figure 16.

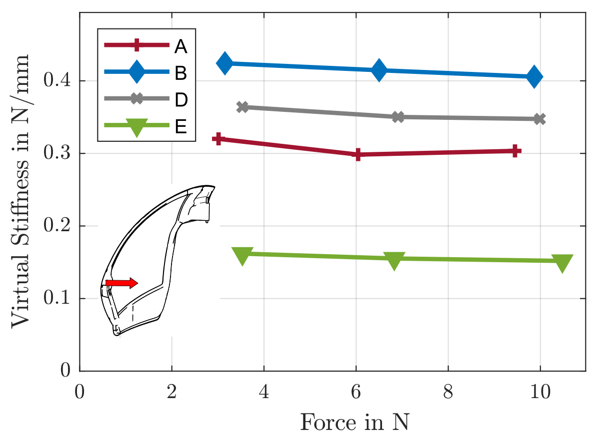

Figure 8: Comparison of virtual stiffness E_v at three load levels applied in +X (inwards)

The results for doors A, B, D and E in -X, equivalent to the direction of opening the cabin door, are shown in figure 9. A similar behaviour as in load case +X is observed with door B being the stiffest of the FFRC cabin doors. Door B requires a force that is 2.6 times larger compared to door E in order to induce a displacement of 1 mm of point P1. No load level 2 is recorded for door E, hence the missing data point, which also applies to load case -Y.

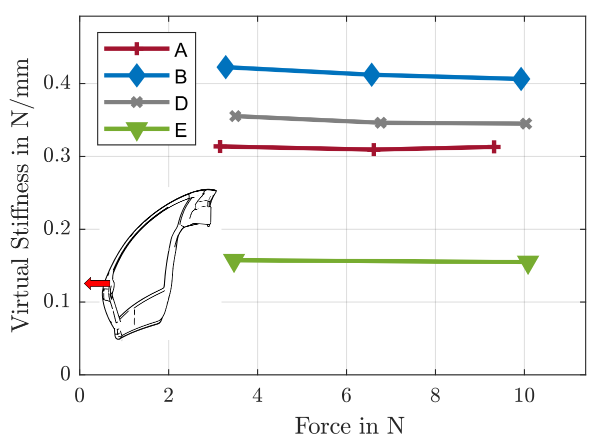

Figure 9: Comparison of virtual stiffness E_v at three load levels applied in -X (outwards)

Figure 10 provides the results for the loads that are applied in +Y, meaning in upwards direction. It can be observed that Bs has the highest E_v, which is around 52 % higher compared to reference C. This is due to the glued-in PMMA window providing more structural stiffness with a higher area moment of inertia. When comparing the doors without window, it can be seen that the FFRC door B and the CFRC door C have a comparable virtual stiffness. Door A and D have a similar E_v for all three load levels with an approximate increase of 100 % compared to door E.

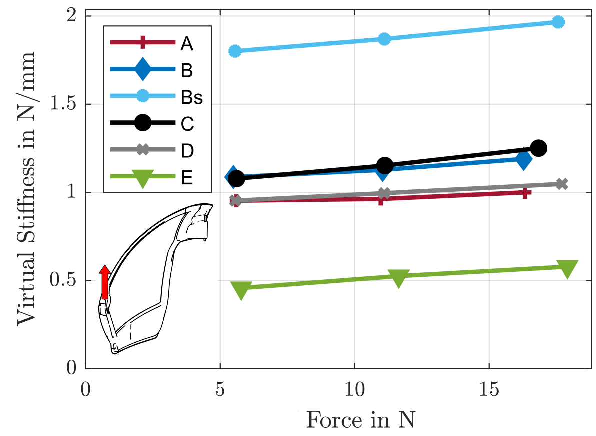

Figure 10: Comparison of virtual stiffness E_v at three load levels applied in +Y (upwards)

In figure 11, the results for -Y in downwards direction show very consistent load application for all load cases between the different doors. This is because the applied weights are directly attached to the door via a cable and pull downwards with no pulley in between. For this load case the FFRC door B shows even a higher E_v compared to the carbon reference door C in black. Door D possesses only a slightly lower stiffness compared to C, followed by door A and door E with the lowest stiffness. Door Bs has again the highest E_v due to the PMMA window.

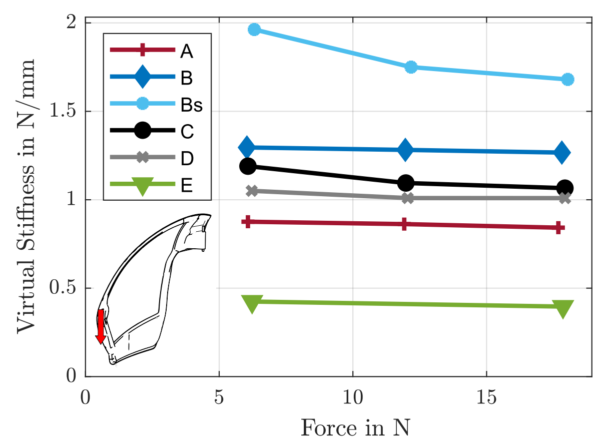

Figure 11: Comparison of virtual stiffness E_v at three load levels applied in -Y (downwards)

Comparing the doors with a load applied in +Z, as shown in figure 12, it can be seen that the window in Bs contributes strongly with the highest virtual stiffness followed by the CFRP reference door C. A decrease in E_v when compared to the reference C can be observed for door B with 18 %, followed by 36 % for door D, 47 % for door A and 63 % for E. The virtual stiffness appears to increase linearly with a higher load level except for door C, with a high first value, which needs to be further investigated.

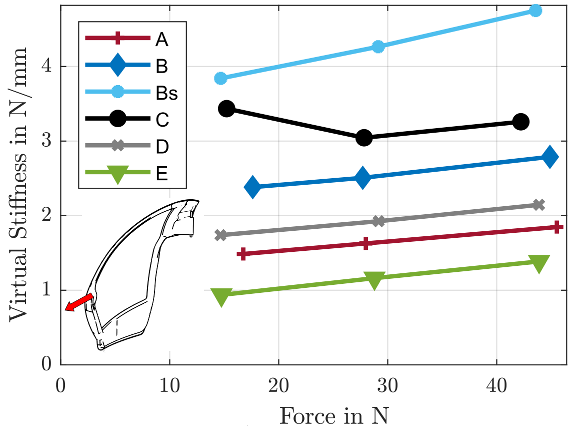

Figure 12: Comparison of virtual stiffness E_v at three load levels applied in +Z (forwards)

Creep recovery in hybrid flax-based composites

The recovery after creep is quantified by recording the resultant displacement of point P1 directly after unloading the last load level L3 as well as recording the displacement after a 10 minutes wait. The results are shown in figure 13 with the recovery of every door after each load case. A negative value means that the resultant displacement is reduced by the given value after the time passed. It can be observed that door Bs in ±X has the highest value, which could be attributed to induced internal stresses and the window glued-in with an elastic adhesive. Doors Bs and C show a positive value for load case +Z, which needs to be further investigated. Doors B, D and E have similar values compared to approximately double the amount of recovery of door A, which also requires further investigation of its origin.

Doors A and B are evaluated regarding the maximum surface strain of the inner and outer shell when applying several virtual strain gauges between the photogrammetric markers. The FFRP material with bio-epoxy produced at 2 bar with approximately 41 % FVC possesses an elongation at break ε_{max} of 1.67 % for UD0 and 1.11 % for BD0/90 with the flax fibers having a yield point between primary and secondary Young's modulus at a strain of 0.17 % for UD and 0.26% for BD. The maximum measured strain at load level L3 on the outer shell is 0.11 % for door A and 0.08 % for door B lying both below the yield point for UD. For the inner shell the maximum recorded strain is 0.195 % for door A and 0.045 % for door B, which is also for both doors below the yield point of BD. As these virtual strain gauges span between two photogrammetric markers they average the strain between them, which means that local maxima can still be higher than these averaged numbers.

Modal analysis results

The frequency response functions of points P1 and P2 with the excitation of point LA in x, y and z measured with DIC system as well as load cell are evaluated. The modeshapes can be visualized in *GOM Correlate*, which helps to assign the natural frequencies and eliminate rigid body modes. The results of the modal analysis are shown in figure 14 with the loss factor as a function of frequency. Only four modeshapes are compared, which reduces the regarded maximum frequency to around 26 Hz. The first modeshape, shown as a cross, is a movement of the point P1 in ±X direction. The second modshape, shown as a diamond shape, is an up- and downwards motion of point P1 in ±Y in combination with a slight torsion around the z-axis. The third modeshape, shown as square, is a torsional movement of the door around the z-axis. The fourth modeshape, shown as dot, is a bending motion with point P1 staying at the z-axis and the middle section of the door moving in ±X direction.

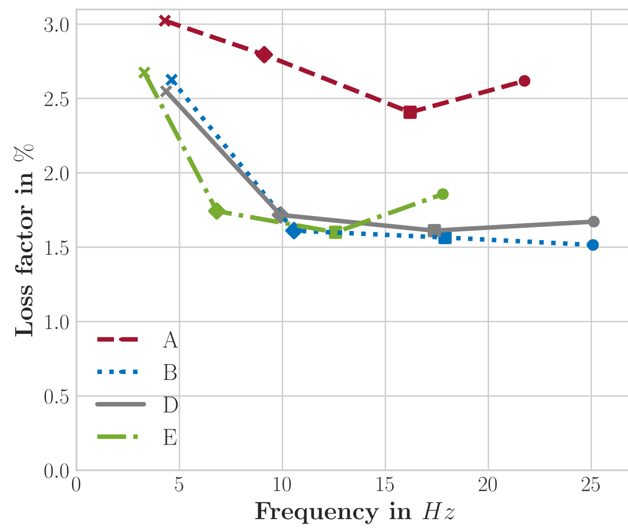

Figure 14: Loss factor as a function of frequency of doors A, B, D and E

The influence of the fixed support needs to be considered when evaluating the loss factor η, which can be here seen at the high η at the first eigenfrequency. Due to a thinner hinge pin and a challenging torsional clamping for doors Bs and C, the data is not considered for the evaluation in figure 14. Doors B and D have very similar loss factors at nearly the same eigenfrequencies of around 1.6 % for mode 2-4. Door E has similar loss factors however at lower eigenfrequencies for modes 1-4, which corresponds to the lower virtual stiffness compared to the other doors. With doors A and E having the same geometry, it can be noticed that the loss factor of the fourth eigenmode is increasing compared to the third. Door A is made from the same materials as doors B and D, however with 21 % less carbon fibers. This could contribute to its higher loss factor as well as uneven matrix distribution and a higher porosity of the material.

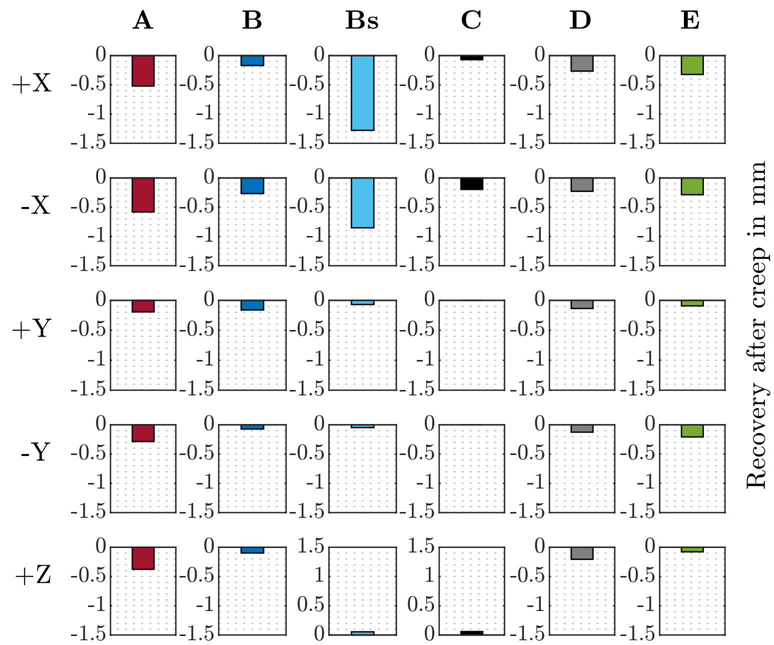

Figure 13: Recovery after creep in millimeters within 10 minutes after unloading

Limitations

For the static structural tests, the applied force varies slightly throughout the tests due to friction in the pulley. For this reason, the load cell is used to measure the applied force excluding inaccuracies in the force determination.

A variation of the measurement results could arise due to the fact that the photogrammetric markers are positioned manually onto the structure. However, due to the comparatively large lever of point P1 on the door, this can be neglected.

For the dynamic measurement, the DIC system has limitations regarding frame rate and computer memory, which influences the bandwidth and frequency resolution of the FRFs.

For the initial measurements, a speckle pattern was applied on the surfaces near the hinge pin and the stress-critical load paths in order to retrieve a continuous strain field under load application. However, due to the large total measuring area and the small expected strain, no relevant data could be obtained. This could be improved with a reduced measuring are and therefore higher resolution. Also, due to the 3D geometry of the area around the hinge pin of the inner shell, not every surface is visible to both camera lenses at the same time, which therefore cannot provide images and hence no strain field data.

Generally, also the production quality and repeatability of the doors regarding fiber volume fraction, even matrix distribution, ply angle and layup precision can have an impact on the results and its comparability.

CONCLUSION AND OUTLOOK

Ecologically sustainable FFRC structures are still in the research stage, but their application in the aviation sector is possible due to their lightweight potential, good mechanical and damping properties. Five hybrid flax fiber-based helicopter cabin doors A, B, Bs, D and E are experimentally compared with the original CFRC reference door C in terms of their static structural performance, modal and damping properties. The cabin doors have a fixed support at the hinge pin with a load cell acting as a wall mount to measure forces and moments in the three axes. The optical measurement with digital image correlation allows to detect the 3D displacement of photogrammetric markers distributed over the cabin door structure. For static measurements, loads are applied to the door handle and the corresponding displacements are recorded. The virtual stiffness of the door structures compares the required resultant force per millimeter of resultant displacement and provides a basis for evaluating different designs. In addition, after the door is impacted with a modal hammer, the 3D displacements are recorded optically at a frame rate of 115 Hz and are used to determine mode shapes and damping characteristics. The following conclusions of this investigations can be drawn:

1. The design of cabin door B with four UD layers in the outer shell and two BD layers in the inner shell shows a similar and for one load case even higher virtual stiffness compared to the pure CFRC reference. This design of door B shows the best structural performance of the FFRC cabin doors with a bio content of 40.5 % and a

higher mass of 29.7 % compared to the reference. The design of door D with only three UD layers in the outer shell resulted in a slightly lower but comparable structural stiffness compared to reference C with a bio content of 40.8 % and a 22.3 % higher mass.

2. The bio-based contents of doors A, B, Bs and D are between 40.5 - 41.8 % with a relatively low FVC of about 41 % due to the curing cycle at 2 bar autoclave pressure. By improving the FVC to 50 % with the help of a higher autoclave pressure of 5 bar and with the use of an epoxy resin with bio-based share > 40 %, a total bio-based content of the structure (inner and outer shell plus adhesive) of > 50 % can be projected.

3. With the possible higher FVC of 50 %, the weight penalties of doors B and D compared to the reference can be reduced to 19.5 % and 12.8 %, respectively.

4. The new flax prepreg materials with bio-epoxy resin and optimized design of doors A, B, Bs and D significantly improved the virtual stiffness by 50 -200 % compared to the first design of door E of the previous project.

5. High damping with loss factors between 1.5 - 3 % could be determined of the flax fiber structures. However, the influence of the fixed support at the hinge pin needs to be considered.

As a further research, the effect of tempering process on FFRCs can be evaluated for tensile stress σ_{22} and shear stress τ_{12} for UD and BD. Also, the loss factor can also be evaluated in more detail with respect to strain dependencies as well as boundary conditions. In addition, the strain field measurement of the speckle pattern at the critical load paths of the structure can be performed with the appropriate optical lenses of the DIC system to obtain higher resolution data.

Author contact:
Lukas Gaugelhofer, lukas.gaugelhofer@tum.de

ACKNOWLEDGMENTS

This research is conducted within in the scope of the joint research project *InteReSt II* of the Luftfahrtforschungsprogramm (LuFo VI-1) with Chemnitz University of Technology (Department of Lightweight Structures and Polymer Technology) and Hanover University of Applied Sciences and Arts (Institute for Bioplastics and Biocomposites) with the funding of the Federal Ministry of Economic Affairs and Climate Action of the Federal Republic of Germany. Moreover, Claudius Breitmoser contributed to the experiments within the scope of his bachelors' thesis.

Federal Ministry
for Economic Affairs
and Climate Action

REFERENCES

1. Nilmini P.J. Dissanayake, J. Summerscales, S. M. Grove, and M. M. Singh. *Energy use in the production of flax fiber for the reinforcement of composites.* Journal of Natural Fibers, 6(4):331–346, 2009.

2. Dittenber, D., and Gangarao, H., *Critical review of recent publications on use of natural composites in infrastructure.* Composites Part A, 43:1419–1429, 2012.

3. Ashby, M.F., *Materials and the Environment: an eco-informed material choice.* Butterworth-Heinemann/Elsevier, 2nd edition, 2013.

4. Madsen, B., and Lilholt, H., *Guidelines for mechanical design with biocomposites: properties, weight and cost.* JEC Magazine, 37, 2007.

5. Wernet, G., Bauer, C., Steubing, B., Reinhard, J., Moreno-Ruiz, E., and Weidema, B., *The ecoinvent database version 3 (part I): overview and methodology.* The International Journal of Life Cycle Assessment, 21(9):1218–1230, 2016.

6. Bos, H. L., *The potential of flax fibres as reinforcement for composite materials.* PhD thesis, Technische Universiteit Eindhoven, 2004.

7. Genc, G., El Hafidi, A., and Gning, P. B., *Comparison of the mechanical properties of flax and glass fiber composite materials.* Journal of Vibroengineering, 14(2):572–581, 2012.

8. John, J., Gaugelhofer, L. and Hajek, M., *Increasing Damping Properties of Carbon Laminates by Flax Fiber Hybridization for Rotorcraft.* 48th European Rotorcraft Forum, Winterthur, 2022.

9. Karus, M., Kaup, M., and Lohmeyer, D., *Study On Markets and Prices for Natural Fibres (Germany and EU).* Technical Report March, nova Institute, Hürth, Germany, 2000.

10. Karus, M.; Kaup. M.; *Naturfasern für die europäische Automobilindustrie.* Nova-Insti-tut, 2002 URL: http://nova-institut.de/pdf/studie-naturf-auto.pdf

11. Strohrmann, K., *Biocomposites in Aviation Structures on the Example of Flax and its Hybrids.* PhD thesis, Technische Universität München, 2019.

12. John, J., Gaugelhofer, L. and Hajek, M.,Yavrucuk, I., *Increasing Damping Properties of Helicopter Composite Substructures using Flax Fiber Hybridization.* Vertical Flight Society's 79th Annual Forum and Technology Display, West Palm Beach, FL, USA, May 16-18, 2023.

13. Gaugelhofer, L., John, J. and Hajek, M.,Yavrucuk, I., *Influence of Temperature and Humidity on Flax Fiber-Reinforced Composites for Helicopter Structures Using Protective Coatings*. Vertical Flight Society's 79th Annual Forum and Technology Display, West Palm Beach, FL, USA, May 16-18, 2023.

14. Gaugelhofer, L., John, J. and Hajek, M., *Experimental Investigation of Tensile Properties of Flax Fibre-Reinforced Composites*. 48th European Rotorcraft Forum, Winterthur, 2022.

15. Strohrmann, K., *Abschlussbericht der TUM Arbeitspakete im LUFO V2 geförderten Projekt InteReSt (FKZ: 20E1501C)*. Technical report, Technichal University of Munich, Garching, 2019.

16. Strohrmann, K., Hajek, M.,"An Eco-Efficient Helicopter Tailplane Hybridized from Flax, Balsa and Carbon". AIAA SciTech, San Diego, CA, USA, 2019.

17. Henschel, K., *Biocomposites in Aviation Structures on the Example of Flax and its Hybrids*. Technical University Munich, 2020, DOI: 10.14459/2019 md1488689 .

18. Strohrmann, K., et al.,"Crashworthiness Characteristics of Carbon-Flax Composite Tubes for Aerospace Applications". ECCM18 -18th European Conference on Composite Materials, Athens, Greece, 2018.

19. Strohrmann, K., et al.,*Hybrid Natural Fiber Composites in a Helicopter Cabin Door – Mechanical Properties and Ecological Efficiency*. VFS International 75th Annual Forum & Technology Display, Philadelphia, 2019.

20. Strohrmann, K., et al.,*Bilinear Approach to Tensile Properties of Flax Composites in Finite Element Analyses*. Journal of Materials Science, 54:1409–1421, 2019.

21. Svidler, Rostislav, and R. Rinberg. *Bio-based hybrid cabin door of ultralight helicopter with variable-axis fiber design*. CEAS Aeronautical Journal (2022): 1-11.

22. DIN EN 2561, *Luft- und Raumfahrt - Kohlenstoffaserverstärkte Kunststoffe - Unidirektionale Laminate - Zugprüfung parallel zur Faserrichtung*. Deutsche Fassung EN 2561:1995

23. DIN EN 2597, *Luft- und Raumfahrt - Kohlenstoffaserverstärkte Kunststoffe; unidirektionale Laminate - Zugversuch senkrecht zur Faserrichtung*. Deutsche Fassung EN 2597:1998

24. DIN EN 6031, *Luft- und Raumfahrt - Faserverstärkte Kunststoffe - Prüfverfahren - Bestimmung der Schubeigenschaften (45-Zugversuch)*. Deutsche und Englische Fassung EN 6031:2015

25. DIN EN ISO 527-4, *Kunststoffe - Bestimmung der Zugeigenschaften - Teil 4: Prüfbedingungen für isotrop und anisotrop faserverstärkte Kunststoffverbundwerkstoffe (ISO 527-4:2021)*. Deutsche Fassung EN ISO 527-4:2021

26. Blok, R., Smits, J., Gkaidatzis, R., and Teuffel, P., *Bio-based composite footbridge: design, production and in situ monitoring*. Structural Engineering International, 29(3), 453-465, 2019.

27. Xu, B., Van Den Hurk, B., Lugger, S. J., Blok, R., and Teuffel, P., *Creep analysis of the flax fiber-reinforced polymer composites based on the time–temperature superposition principle*. Science and Engineering of Composite Materials, 30(1), 20220218, 2023.

28. Robinson, E., and Clark, D., *Sampling and the Nyquist frequency*. The Leading Edge, 10(3), 51-53, 1991

APPENDIX

Figure 15: Carbon fiber-reinforced segments of the inner shell of door B

Figure 16: Geometry differences between door A (left) and door D (right)

Figure 17: Carbon fiber reinforcement of critical load path at outer shell of cabin door B after demolding

Figure 18: PowerRib™ reinforcement of door D outer shell during layup